

A Comparison of Control and Modulation Schemes for Medium-Voltage Drives: Emerging Predictive Control Concepts versus PWM-based Schemes

Tobias Geyer, *Senior Member, IEEE*

Abstract—Control and modulation schemes for AC electrical drives synthesize switched three-phase voltage waveforms that control the electrical machine. Particularly in medium-voltage applications, the aim is to minimize both the switching losses in the inverter as well as the harmonic distortions of the stator currents and the torque. For a given modulation scheme, lower switching losses usually imply higher distortion factors and vice versa. This trade-off can be described by a hyperbolic function, as shown in this paper for pulse width modulation. A number of predictive control concepts are rapidly emerging. Their characteristic hyperbolic trade-off functions are derived, compared with each other, and benchmarked with respect to pulse width modulation and off-line optimized pulse patterns. It is shown that predictive schemes with long prediction horizons shift the performance trade-off curve towards the origin, thus lowering both the switching losses and the harmonic distortions. As a result, at steady-state operating conditions, these predictive schemes achieve a performance similar to optimized pulse patterns, whilst providing a superior dynamic performance during transients.

Index Terms—AC motor drives, medium-voltage drives, control and modulation schemes, model predictive control, pulse width modulation, optimized pulse patterns, performance trade-off

ACRONYMS

DTC	Direct torque control.
FOC	Field oriented control.
IGCT	Integrated gate commutated thyristor.
IM	Induction machine.
MPC	Model predictive control.
MPDCC	Model predictive direct current control.
MPDTC	Model predictive direct torque control.
NPC	Neutral point clamped.
OPP	Optimized pulse pattern.
PD	Phase disposition.
PWM	Pulse width modulation.
SVM	Space vector modulation.
TDD	Total demand distortion.
THD	Total harmonic distortion.

I. INTRODUCTION

Variable speed drive systems based on voltage source inverters consist of an active or passive grid-connected rectification

T. Geyer is currently with the Department of Electrical and Computer Engineering, The University of Auckland, Private Bag 92019, Auckland 1142, New Zealand; tel. number: +64 (9) 373 7599 extension 89634; e-mail: t.geyer@ieee.org

A preliminary version of this paper was published and presented at the ECCE 2010 in Atlanta, USA, with the paper ID 93.

stage, a dc-link with capacitors, a machine-side inverter and an electrical machine. In the medium-voltage domain with power levels exceeding one megawatt, Neutral Point Clamped (NPC) three-level inverters are the standard choice when considering voltage source inverters [1]. For such drives, the two control schemes traditionally employed are Field Oriented Control (FOC) [2] and Direct Torque Control (DTC) [3].

Recently, the power electronics community has started to adopt the concept of Model Predictive Control (MPC) from the control community [4], [5], [6]. The roots of MPC can be traced back to the process industry, where the origins of MPC were developed in the 1970s [7]. Today, MPC is used extensively in industry with several thousand reported applications [8].

Broadly speaking, the emerging field of MPC for electrical drives can be divided into two groups. The first set of approaches builds on FOC by replacing the inner (current) control loop by MPC and keeping the modulator in place. Examples for this include [9] and [10]. In the second variety, MPC directly manipulates the inverter switch positions, thus superseding a modulator. The latter scheme is available with a prediction horizon of length one, see e.g. [11], [12], or with longer prediction horizons encompassing up to 100 time-steps, such as in Model Predictive Direct Torque Control (MPDTC). MPDTC can be considered as an improvement of DTC, where the look-up table is replaced by an online MPC-type optimization stage. MPDTC was developed in early 2004, see [5] and [13], experimentally verified on a 2 MVA drive in 2007 [14] and later generalized to enable even longer prediction horizons [15]. A recently proposed derivative of MPDTC is Model Predictive Direct Current Control (MPDCC) [16], [17].

The first objective of this paper is to review and compare two emerging predictive control methodologies, namely one-step predictive control with reference tracking, and MPC with long prediction horizons and bounds. Both schemes are available as current controllers and as torque and stator flux magnitude controllers. The second objective is to benchmark these predictive schemes with established control and modulation methodologies, namely FOC with Pulse Width Modulation (PWM), Space Vector Modulation (SVM) and Optimized Pulse Patterns (OPPs). At steady-state operating conditions, the key performance criteria are the switching losses in the inverter and the harmonic distortions of the stator current and the torque. The trade-off between the switching

losses and the distortion level is well-known and fundamental to power electronics. As will be shown in this paper, the product of the two is equal to a constant. This constant depends on the chosen control and modulation scheme, thus giving rise to a hyperbolic performance trade-off curve. Through analysis and simulations, the location of these hyperbolas is determined for each scheme. It is shown that long prediction horizons in MPC schemes significantly enhance the performance, whilst overly short horizons might lead to results inferior to PWM.

The comparison is intended to be general and independent from the machine, power rating and semiconductors used. To achieve this, a drive system setup with as few parameters as possible is used, neglecting second order effects such as deadtimes, delays and measurement noise. Specifically, as a case study, a three-level NPC voltage source inverter driving a medium-voltage induction machine is chosen.

The paper is organized as follows. Sect. II states the requirements for control and modulation schemes with regards to MV drives, from which the performance criteria for the comparison are deduced in Sect. III. The hyperbolic performance trade-off curve is derived in Sect. IV for PWM and SVM. Based on the drive system case study presented in Sect. V, four current control schemes are summarized and compared in Sect. VI, namely FOC with PWM/SVM, FOC with OPP, MPDCC and one-step predictive current control. Accordingly, Sect. VII summarizes and compares two predictive torque and flux control schemes, namely MPDTC and one-step predictive torque control. The findings of the comparisons are discussed in Sect. VIII and conclusions are drawn.

II. REQUIREMENTS FOR CONTROL AND MODULATION SCHEMES FOR MEDIUM-VOLTAGE DRIVES

The requirements for control and modulation schemes can be grouped into requirements relating to the machine and requirements relating to the inverter, respectively.

A. Requirements Relating to the Electrical Machine

With regards to the machine, the demanded electromagnetic torque is to be produced, the torque is to be quickly adjusted during load changes, speed transients or faults, and the machine's airgap flux is to be controlled so as to keep the machine appropriately fluxed. The switched voltage waveform of the inverter causes harmonic current distortions that give rise to copper losses and thus to thermal losses in the stator. Since the capability of cooling the rotor is limited, particularly at low speed, the current harmonics have to be kept small.

The mechanical load usually requires a smooth torque. A low harmonic torque distortion corresponds to a small torque ripple that limits the mechanical stress and wear of the shaft, the bearings and the load. Moreover, the risk of exciting torsional eigenmodes of the drive train is minimized, see for example [18] and references therein.

Apart from that, the insulation of the stator winding has to be rated for the resulting dv/dt . The latter mainly depends on the voltage per semiconductor and its switching characteristic (slope) rather than on the modulation scheme.

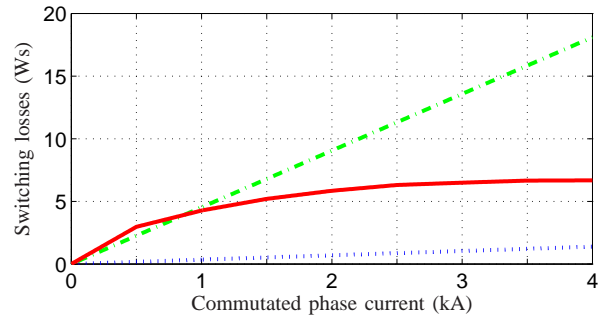


Figure 1: Switching losses as a function of the commutated current for the GCT and the diodes. The GCT turn-on losses are indicated by the dotted blue line, the GCT turn-off losses by the dash-dotted green line, and the reverse recovery losses are the straight red line

B. Requirements Relating to the Inverter

Due to the high currents and voltages in the medium-voltage domain, the semiconductors' switching and conduction losses in the inverter can be substantial. Thermal limitations impose an upper bound on the tolerable losses. An indirect way of minimizing the switching losses is to minimize the switching frequency. Even though the semiconductors are often water cooled in the high power range, the achievable switching frequency with today's available semiconductor devices is typically limited to a few hundred Hz.

For multi-level inverters, additional requirements often arise, such as the balancing of a neutral point potential around zero.

III. PERFORMANCE CRITERIA

From the requirements stated in the previous section, the following three performance criteria are deduced for the comparison: inverter switching losses, harmonic distortions of the stator currents and harmonic distortions of the electromagnetic torque. These criteria refer to steady-state operating conditions. Other possible criteria include the dynamic behavior of the controller, such as the torque settling time during torque steps, the controller's sensitivity to parameter variations and flux estimation errors, etc. These issues are beyond the scope of this paper, which focuses on the steady-state operating regime only.

A. Total Demand Distortion

A suitable measure for the harmonic distortion of the current is the Total Demand Distortion (TDD), which is defined as

$$I_{\text{TDD}} = \frac{\sqrt{0.5 \sum_{h \neq 0} I_h^2}}{I_{\text{nom}}}, \quad (1)$$

where the nominal current I_{nom} refers to the operating condition at nominal speed and full load of the drive. The (harmonic) Fourier components I_h , $h \geq 0$, can be differentiated between the fundamental current component I_0 and the h -th

harmonic amplitude component I_h^1 . The harmonic distortion of the electromagnetic torque is defined accordingly.

B. Switching and Conduction Losses

The switching losses depend on the applied voltage, the commutated current and the semiconductor characteristics. Considering Integrated Gate Commutated Thyristors (IGCTs), with the GCT being the semiconductor switch, the switch-on and switch-off losses can be considered to be linear in the dc-link voltage and the phase current. For a diode, the switch-on losses are effectively zero, while the turn-off losses—the reverse recovery losses—are again linear in the voltage, but nonlinear in the commutated phase current.

Observing that in an NPC inverter the voltage seen by each semiconductor is always half the total dc-link voltage V_{dc} leads to the following turn-on (energy) loss of the i -th GCT.

$$E_{i,on} = e_{on} \frac{1}{2} V_{dc} |i_{ph}|, \quad (2)$$

where e_{on} is a GCT specific coefficient and i_{ph} is the phase current. For the GCT turn-off and diode reverse recovery losses, similar equations can be derived.

As shown in [15], [19], by inspecting the phase leg topology and the commutation paths, the switching (energy) losses per phase transition can be derived. Since the commutation depends on the polarity of the phase current, the cases with positive and negative phase current need to be treated separately. Summing up the switching (energy) losses in the individual semiconductor devices (with the unit Ws) and dividing them by the elapsed time yields the average switching (power) losses P_{sw} for the inverter (with the unit W).

Using the 35L4510 4.5 kV 4 kA IGCT and the 10H4520 fast recovery diode as examples both from ABB, the device switching losses as a function of the commutated current are depicted in Fig. 1 assuming $0.5V_{dc} = 2600$ V and a nominal operating temperature.

For GCTs the switching losses significantly exceed the conduction losses, particularly at low switching frequencies. Moreover, for NPC inverters the conduction losses can be considered to be independent from the switching pattern and thus from the modulation scheme in use. Hence, the conduction losses are not included in the performance evaluation and not addressed in the controller objective function.

IV. PERFORMANCE TRADE-OFF FOR PWM/SVM

For a given operating point (fundamental frequency, machine voltage and load torque) consider the TDD of the stator

¹Note that the nominal current is an rms value, while the harmonic amplitudes are peak values. The factor 0.5 is required to translate these peak values into rms values. Moreover, the above definition holds for a single-phase current only. To compute the TDD of a three-phase current, the TDD is computed for each a , b and c current component separately, and the overall TDD is determined by taking the mean value of the three. The TDD is a more suitable means to express the harmonic distortion than the Total Harmonic Distortion (THD), which is defined similarly to (1), but is referred to the fundamental waveform of the instantaneous current rather than to the fundamental of the nominal current. As a result, for small current amplitudes, the THD tends to go to infinity, while the TDD remains effectively constant.

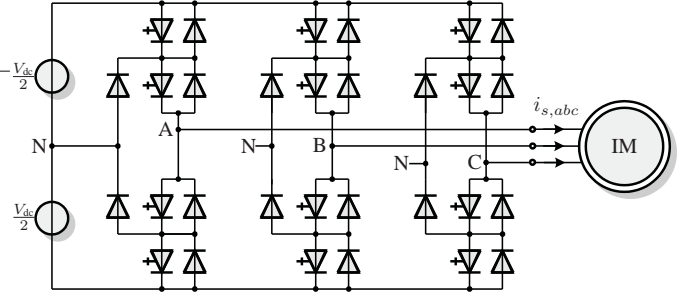


Figure 2: Three-level neutral point clamped voltage source inverter driving an induction motor with a fixed neutral point potential

currents $I_{s,TDD}$ and the switching losses of the inverter P_{sw} . The two quantities give rise to a trade-off that is fundamental to power electronics. Specifically, for a given modulation method, it is well known in a qualitative manner that reducing $I_{s,TDD}$ leads to a higher P_{sw} and vice versa. This trade-off can be also established in a quantitative way as done hereafter, namely that the product of the two quantities is equal to a constant. This implies that reducing $I_{s,TDD}$ by a certain percentage increases P_{sw} by the same amount. This constant characterizes the steady-state performance of the considered modulation scheme. In [20], a similar figure of merit was introduced, which is the product of the spectral amplitudes and the switching frequency. This section extends this concept by considering the switching losses, which appear to be of more imminent importance to the inverter operation than the switching frequency,

Consider a carrier-based modulator with the carrier frequency f_c and the fundamental frequency f_0 . It is well known that the resulting harmonics are located at the frequencies [21]

$$f_{h,mn} = mf_c + nf_0, \quad m, n \in \mathbb{N} \quad (3)$$

and that the amplitudes of the harmonic current components are equal to the voltage amplitudes $V_{h,mn}$ divided by the impedance of the total leakage inductance L_σ of the machine.

$$I_{h,mn} = \frac{V_{h,mn}}{2\pi f_{h,mn} L_\sigma}. \quad (4)$$

For frequencies sufficiently higher than the fundamental frequency, (4) can be approximated as

$$I_{h,mn} \approx \frac{V_{h,mn}}{2\pi m f_c L_\sigma}. \quad (5)$$

The latter approximation is fairly accurate, since the sidebands nf_0 around the carrier frequencies mf_c quickly approach zero as n increases, and since the carrier-to-fundamental frequency ratio is typically $f_c/f_0 \geq 12$. As a result, the amplitudes of the current harmonics are inversely proportional to the carrier frequency, i.e. $I_{h,mn} \sim 1/f_c$. The same applies to the current TDD, i.e. $I_{s,TDD} \sim 1/f_c$, as can be seen from (1).

For the i -th semiconductor with the corresponding phase current i_{ph} , consider the turn-on switching losses over one fundamental period T_0 . Using (2) the turn-on losses are given

Induction Motor			
Voltage	3300 V	r_s	0.0108 pu
Current	356 A	r_r	0.0091 pu
Real power	1.587 MW	x_{ls}	0.1493 pu
Apparent power	2.035 MVA	x_{lr}	0.1104 pu
Frequency	50 Hz	x_m	2.3489 pu
Rotational speed	596 rpm		
Inverter			
Dc-link voltage	5200 V	V_{dc}	1.930 pu

Table I: Rated values (left) and parameters (right) of the drive

by

$$P_{i,on} = \frac{1}{T_0} \sum_{\ell=1}^{\ell_{on}} E_{i,on}(\ell) = \frac{1}{2} V_{dc} \frac{e_{on}}{T_0} \sum_{\ell=1}^{\ell_{on}} |i_{ph}(\ell)|, \quad (6)$$

where ℓ_{on} denotes the number of turn-on events for this device per T_0 . When operating in the linear modulation regime, the pulses generated by the PWM are effectively equally distributed over the fundamental period. This implies $i_{ph}(\ell) \approx \hat{i}_{ph} \sin(2\pi \frac{\ell}{\ell_{on}})$ for $\ell = 1, \dots, \ell_{on}$ with \hat{i}_{ph} denoting the peak current of the fundamental waveform, neglecting the ripple current. Since $\ell_{on} \sim f_c$ it directly follows that $P_{i,on} \sim f_c$. The same applies to the turn-off and reverse recovery losses. Thus, also the total switching losses are proportional to the carrier frequency, i.e. $P_{sw} \sim f_c$, leading to the statement

$$I_{s,TDD} \cdot P_{sw} = \text{const}. \quad (7)$$

Due to the equivalence shown in [22], the same applies to Space Vector Modulation (SVM), but not necessarily to OPPs, since their pulses are often not equally distributed over time.

V. DRIVE SYSTEM CASE STUDY

To compare different control and modulation schemes with each other a drive system case study needs to be chosen. This case study should be as general as possible to ensure that the benchmarking results are meaningful and sufficiently general to be of value. Moreover, the comparison is intended to focus on the core performance behavior and characteristic of the different control and modulation methods to establish the theoretical baseline performance. To achieve this, it is beneficial to neglect non-idealities and second order effects that typically arise in a real-world drive setting, as summarized in [23]. In an industrial controller implementation, well-known schemes are readily available to mitigate and compensate for these effects to a large extent—this applies equally to traditional schemes as well as to emerging predictive control and modulation methods.

A. Assumptions

The assumptions made for the drive system case study include the following.

- Dc-link: an idealized dc-link with two constant dc-link voltage sources (without any voltage ripple) is assumed, making an active balancing of the neutral point obsolete.
- Inverter: the deadtime between the commutation command and the actual commutation of the current is

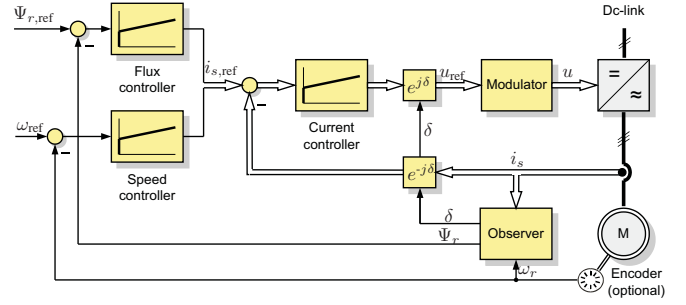


Figure 3: Field oriented control with a pulse width or space vector modulator

neglected, as well as any jitter, interlocking times, and minimum on and off times for the semiconductors. Note, however, that the switching losses are taken into account, see Sect. III-B.

- Electrical machine: the magnetic material is assumed to be linear (saturation neglected), the stator resistance is constant, the skin effect in the rotor is neglected and harmonics due to the arrangement of the windings in discrete slots are not considered.
- Controller: the delay between the sampling instant and the control output due to the controller's computation time is not considered.
- Measurements: the voltage, current and speed measurements and/or estimates are assumed to be ideal without gain errors, offsets and measurement noise.
- Load: the mechanical load is assumed to be constant.

B. Drive System Setup

As a case study, consider a three-level neutral point clamped voltage source inverter with an induction machine, as shown in Fig. 2. In the arena of medium-voltage drives, this drive configuration is the one most commonly used.

As has already been indicated in Sect. III-B, the inverter's total dc-link voltage is $V_{dc} = 5.2$ kV. ABB's 35L4510 4.5 kV 4 kA IGCT and ABB's 10H4520 fast recovery diode constitute the semiconductors with the switching loss profile shown in Fig. 1. Switching between the upper and the lower rail is prohibited to avoid a shoot through, but all other transitions are allowed. A 3.3 kV and 50 Hz squirrel-cage induction machine rated at 2 MVA is used as an example for a commonly used medium-voltage induction machine. A summary of the machine and inverter parameters can be found in Table I.

All simulations were run at the same operating point at 60% speed with a 100% torque setpoint.

VI. CURRENT CONTROL SCHEMES

A. FOC with PWM/SVM

As shown in Fig. 3, FOC is formulated in an orthogonal reference frame rotating synchronously with the stator or rotor flux. Two (orthogonal) control loops are used—one for the flux and one for the torque producing current. A subsequent Pulse Width or Space Vector Modulator (PWM or SVM) translates the stator voltage reference signals into gating commands for

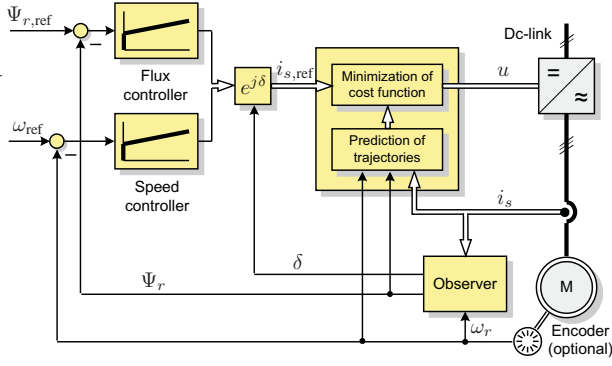


Figure 4: Predictive direct current control

the inverter [20]. A three-level regular sampled PWM is used with two triangular carrier signals, which are in phase (phase disposition). It is generally accepted that for multi-level inverters carrier-based PWM with phase disposition (PD) results in the lowest harmonic distortion. As shown in [22]—by adding an appropriate common mode voltage to the reference voltage, which is of the min/max plus modulo type—PWM with PD is equivalent to SVM, in the sense that both methods yield the same gating signals.

In simulations based on the above case study at 60% speed and rated torque, the carrier frequency was varied between 150 Hz and 1.2 kHz. Synchronous PWM was used, with the carrier frequency being integer multiples of the fundamental frequency. After reaching steady-state operating conditions, the machine currents, voltages and the torque were recorded, and the switching losses P_{sw} were computed according to Sect. III-B. The current and torque TDDs were computed using Fourier transformations over integer multiples of the fundamental period. The TDDs were normalized with respect to rated conditions, while the switching losses were normalized using the rated apparent power S_{rat} .

Figs. 5(a) and 5(d) show the resulting harmonic distortions of the stator currents and the torque as a function of the normalized switching losses of the inverter. The individual simulations are denoted by (blue) stars that, as anticipated in Sect. IV, can be approximated by hyperbolic functions of the form²

$$I_{s,TDD} \cdot \frac{P_{sw}}{S_{rat}} = 1.3, \quad T_{s,TDD} \cdot \frac{P_{sw}}{S_{rat}} = 0.55. \quad (8)$$

This implies that when reducing the PWM carrier frequency so as to reduce the switching losses, e.g. by 50% percent, the current and torque TDDs are increased by 50% and vice versa.

Note that predictive schemes such as [9] and [10] that replace the inner current control loop by MPC, but keep the PWM modulator in place, lead to the same steady-state performance metrics.

²A small offset in the switching losses of 0.02% is neglected here that accounts for the fact that the switching losses cannot be made zero since some switching is always required to synthesize the fundamental waveform.

B. FOC with OPP

Alternatively, OPPs can be calculated in an off-line procedure by computing the optimal switching angles over one fundamental period for all possible operating points [24]. For a given switching frequency (pulse number), the optimization criteria is the minimization of the weighted voltage distortion, which is approximately equal to the current distortion. OPPs are typically used in very slow control loops such as V/f control or in non-aggressively tuned FOC loops.

Figs. 5(a) and 5(d) show the resulting harmonic distortions versus the switching losses, where the individual simulations are denoted by (red) circles.

C. Model Predictive Direct Current Control Problem

By replacing in the FOC setting the inner current control loop and its modulator by an online optimization stage, the current control and the modulation problems can be addressed together, see Fig. 4. Symmetrical bounds around the current references are introduced. The width of the bounds directly determines the current ripple, which in turn is proportional to the current TDD [17]. The control objectives are then to keep the instantaneous currents within the imposed bounds and to minimize the switching losses. The bound width is the tuning parameter that sets the trade-off between the switching losses and the current distortion.

The predictive controller is endowed with a discrete-time model of the drive that enables it to predict the impact of its decisions. The control objectives are mapped into an objective function that yields a scalar cost (here the short-term switching losses) that is to be minimized. At every time-step, the MPC controller computes a sequence of switch positions over a certain time-interval, the prediction horizon, that entails the minimal switching losses over this interval. Out of this sequence, at the current time-instant only the first gating signal is applied to the drive. At the next sampling instant, new measurements are obtained, and the optimization step is repeated, thus providing feedback.

Writing the above control problem as a closed-form optimization problem leads to

$$J^*(x(k)) = \min_{U(k)} \frac{1}{N_p} \sum_{\ell=k}^{k+N_p-1} E_{sw}(x(\ell), u(\ell), u(\ell-1)) \quad (9a)$$

$$\text{s. t. } x(\ell+1) = Ax(\ell) + Bu(\ell) \quad (9b)$$

$$y(\ell) = Cx(\ell) \quad (9c)$$

$$y(\ell) \in \mathcal{Y}(\ell) \quad (9d)$$

$$u(\ell) \in \{-1, 0, 1\}^3, \max |\Delta u(\ell)| \leq 1 \quad (9e)$$

$$\forall \ell = k, \dots, k + N_p - 1, \quad (9f)$$

with $J^*(x(k))$ denoting the minimum of the objective function J as a function of the state vector $x(k)$ at the current time-instant k . It is convenient to use the stator currents i_s and the rotor flux vector ψ_r represented in the $\alpha\beta$ reference frame as state vector x . The motor speed is assumed to be constant within the prediction horizon and is thus not part of the state vector but rather a parameter in the machine model (9b). The

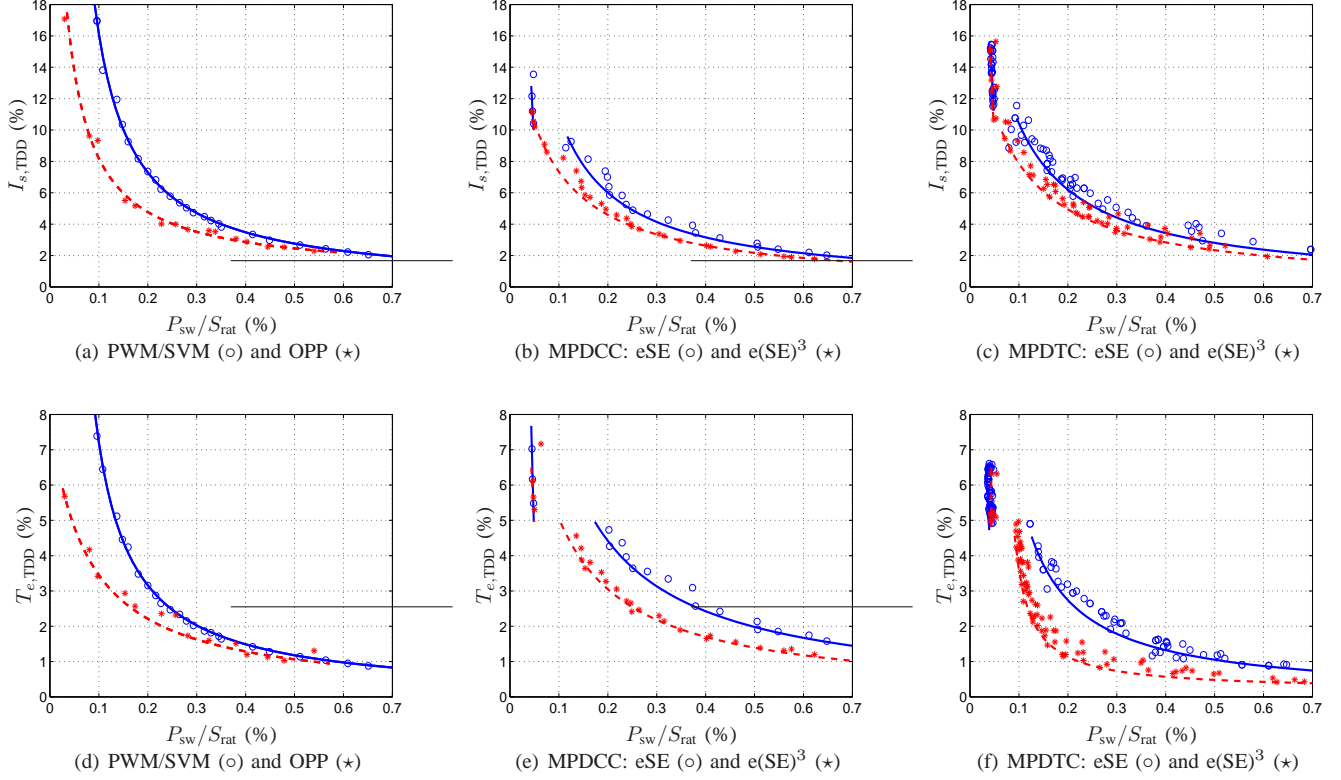


Figure 5: Performance trade-off for FOC with PWM/SVM, FOC with OPP, and long-horizon model predictive direct current (MPDCC) and torque (MPDTC) control. The upper (lower) row shows the current (torque) TDD versus the normalized switching losses

sequence of control inputs $U(k) = [u(k), \dots, u(k + N_p - 1)]$ over the prediction horizon N_p represents the sequence of inverter switch positions the controller has to decide upon. The objective function represents the sum of the switching energy losses over the prediction horizon divided by the horizon length—it thus approximates the short-term average switching power losses. Note that the instantaneous switching energy loss E_{sw} at time-instant ℓ is a function of the stator current $i_s(\ell)$, which is part of the state vector $x(\ell)$. E_{sw} also depends on the inverter switching transition at time-step ℓ , which can be deduced from $u(\ell)$ and $u(\ell-1)$. An indirect (and less effective) way of minimizing the switching losses is to minimize the number of commutations, i.e. the device switching frequency.

The objective function is minimized subject to the dynamical evolution of the drive represented in state-space form with the matrices A , B and C , which are of appropriate form [5], [17]. In this case, the drive's output vector y represents the stator currents i_s , which are to be kept within their respective bounds given by the set $\mathcal{Y}(\ell)$. The constraint (9e) limits the control input u to the integer values $\{-1, 0, 1\}$ available for a three-level inverter. Switching between the upper and the lower rail is inhibited by the second constraint in (9e) with $\Delta u(\ell) = u(\ell) - u(\ell-1)$. These constraints have to be met at every time-step within the prediction horizon.

D. Model Predictive Direct Current Control

Solving the closed-form optimization problem (9) is challenging from a computational point of view even for prediction horizons of modest length. Solving it for reasonably long horizons appears to be impossible³. Since this is a mixed-integer programming problem, it is well-known that in the worst case all 12^{N_p} switching sequences need to be enumerated and evaluated to find the optimum within the sampling interval.

One attractive solution is to consider switching transitions only when the outputs y are close to their respective bounds \mathcal{Y} , i.e. when switching is imminently required to keep the outputs within their bounds. When the outputs are well within their bounds, the switch positions are frozen and switching is not considered. This is in line with the control objective (9a) and greatly reduces the number of switching sequences to be evaluated and thus the computational burden.

To achieve this, three key concepts were introduced in [5], [13], [15], [17] that characterize Model Predictive Direct Current Control (MPDCC).

- 1) The formulation of the optimization problem in an *open form*. For every admissible switching sequence the

³For a given switch position $u(\ell)$, the number of admissible future switch positions $u(\ell+1)$ for a three-level inverter is on average 12 and thus less than 27 due to (9e). Nevertheless, for $N_p = 75$ for example, the number of possible switching sequences U amounts to $12^{N_p} = 10^{80}$, which is equal to the estimated number of atoms in the observable universe.

corresponding output trajectories are computed forward in time.

- 2) Between the switching events, the output trajectories are computed using the model (9b) and (9c), to which we refer as an *extension* step, or they are extrapolated in an approximate manner, which is a so called *extrapolation* step. Typically, quadratic extrapolation is used, even though linear extrapolation is often sufficiently accurate, particularly at low speed.
- 3) The set of admissible switching sequences is controlled by the so called *switching horizon*, which is composed of the elements 'S' and 'E' that stand for 'switch' and 'extrapolate' (or more generally 'extend'), respectively.

It is important to distinguish between the *switching* horizon, i.e. the number of switching instants within the horizon or equivalently the degrees of freedom, and the *prediction* horizon, i.e. the number of time-steps MPC looks into the future. Between the switching instants, the switch positions are frozen and the drive behavior is extrapolated until a hysteresis bound is hit. The concept of extrapolation gives rise to long prediction horizons (typically 30 to 100 time-steps), whilst the switching horizon is very short (usually one to four). For more details about MPDCC, the reader is referred to [13], [15], [17].

Figs. 5(b) and 5(e) depict simulation results for the switching horizons 'eSE' and 'eSESESE', respectively, when varying the current bounds and setting the controller sampling interval to $T_s = 25 \mu\text{s}$. At higher switching losses, the envelope of the points can be again described by a hyperbolic function. Yet, when approaching effectively six-step operation represented by the almost vertical line, the nonlinear behavior of MPC with bounds is revealed.

E. One-Step Predictive Current Control

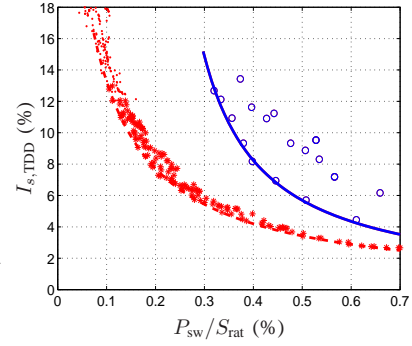
The optimization problem (9) can be greatly simplified by setting the bound width to zero, the prediction horizon N_p to one and minimizing the number of commutations over one time-step only [11]. This scheme operates in the stationary $\alpha\beta$ reference frame and regulates the α and β current components along their references. A tuning parameter λ_n is used to adjust the trade-off between tracking accuracy and switching effort, namely the number of switch transitions.

$$J^*(x(k)) = \min_{u(k)} \|i_e(k+1)\|_1 + \lambda_n \|\Delta u(k)\|_1 \quad (10a)$$

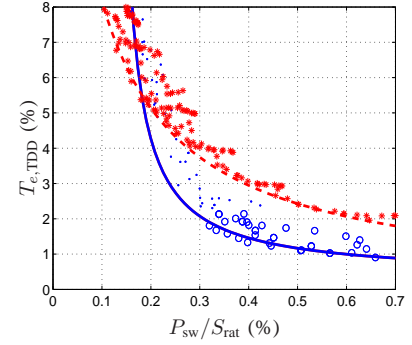
$$\text{s. t. } i_s(k+1) = A_1 i_s(k) + A_2 \psi_r(k) + B u(k) \quad (10b)$$

$$u(k) \in \{-1, 0, 1\}^3, \max |\Delta u(k)| \leq 1 \quad (10c)$$

As previously, the state vector x is composed of the stator currents i_s and the rotor flux vector ψ_r in the $\alpha\beta$ reference frame. The objective function penalizes the predicted current error i_e at the next time-step $k+1$, which is given by the difference between the reference current and the current predicted through the machine model (10b) when applying



(a) Torque (o) and current (*) control



(b) Torque (o) and current (*) control

Figure 6: Performance trade-off for 1-step predictive current and torque control. The upper (lower) plot shows the current (torque) TDD versus the normalized switching losses

$u(k)$, i.e. $i_e(k+1) = i_{s,\text{ref}}(k+1) - i_s(k+1)$ ⁴. Since a prediction horizon of length one is used, the resulting switching frequency could be as high as $T_s/2$.

Similar to the above, hundreds of simulations were performed at steady state. In these, the parameter λ_n was varied between 0 and 0.5, and the controller sampling interval was set between $25 \mu\text{s}$ and 1ms , where the range between 100 and $500 \mu\text{s}$ appears to yield the best results. As shown in Fig. 6, the trade-offs between the distortion levels and the normalized switching losses are again bounded by hyperbolic functions, yet the curves seem to be shifted along the horizontal axis.

VII. TORQUE AND FLUX CONTROL SCHEMES

A. Model Predictive Direct Torque Control

Instead of the stator currents, the torque and flux can be directly controlled in a DTC fashion by manipulating the inverter switch positions, see Fig. 7. As in DTC, the torque

⁴Note that in [11], an RL load with a back EMF is used instead of an electric machine. Accordingly, the back EMF is used instead of the rotor flux in (10b). Moreover, the constraint $\max |\Delta u(k)| \leq 1$ does not appear to be enforced in [11] thus potentially giving rise to shoot-throughs. Apart from that, the objective function might turn out to not be a particularly effective choice, since the controller tends to become unstable even at relatively small λ_n as λ_n is increased. In the case investigated here, when setting $T_s = 100 \mu\text{s}$, for $\lambda_n \geq 0.08$ large current excursions occur. When the penalty on switching outweighs the *relative* reduction of the tracking error, switching is avoided altogether regardless of the *absolute* tracking error. This effect seems to be reflected in Fig. 9 in [11].

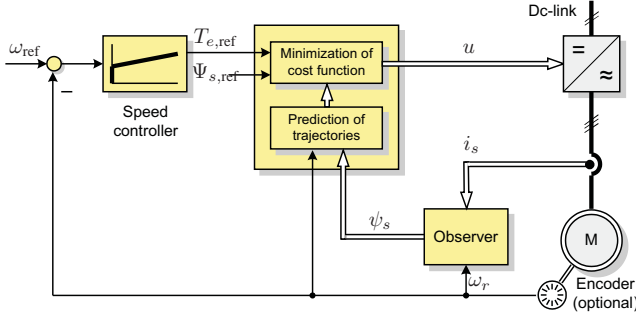


Figure 7: Predictive direct torque control

and stator flux magnitude are kept within pre-specified bounds. Specifically, MPDCC can be translated into a Model Predictive Direct Torque Control (MPDTC) problem by assigning the torque and stator flux magnitude as the output vector y , and by replacing (9c) by $y(\ell) = g(x(\ell))$, where g is a nonlinear function of the state vector. In (9d) \mathcal{Y} denotes then the set defined by the upper and lower torque and flux bounds. In MPDTC, the machine's state vector x is often chosen to comprise the stator and rotor flux vectors in $\alpha\beta$. The algorithmic solution approach to the modified version of the optimization problem (9) is exactly the same as outlined in Sect. VI-D.

For an in-depth description of MPDTC, the reader is referred to [5], [13] and [15]. MPDTC, like MPDCC, is a very versatile concept, and it takes only very little effort and time to adapt it to other inverter topologies, machines and problem setups. Notably, MPDTC has been reported for a five-level inverter composed of three NPC H-bridges [25], PM synchronous machines [26] and drives with LC filters [19].

Figs. 5(c) and 5(f) depict simulation results for various combinations of torque and flux bounds for the switching horizons 'eSE' and 'eSESESE', respectively. The envelope of the points can again be described by hyperbolic functions. Due to the arbitrary selection of the various bounds through simple gridding, many points lie far away from this envelope, are thus suboptimal and not shown here. Unlike in the other trade-off plots in this paper, each simulation point in Fig. 5(c) does not necessarily correspond to a point in Fig. 5(f). Specifically, to achieve the very low torque TDDs for MPDTC with 'eSESESE', the current TDD tends to get somewhat compromised, namely for a given switching loss on the horizontal axis, the point that minimizes the torque TDD does not, in general, also minimize the current TDD. The converse is also true, yet less pronounced, in the sense that minimal current TDDs also yield close to optimal torque TDDs that are similar to the torque TDDs achieved by the OPPs.

B. One-Step Predictive Torque Control

Similarly to Sect. VI-E, the optimization problem can be simplified by setting the bound widths to zero, the prediction horizon to one and minimizing the number of commutations

over one time-step [12]⁵. This scheme also operates in the stationary reference frame, but regulates the torque and stator flux magnitude along their references. The objective function penalizes the squared sum of the output variables y . The tuning parameter λ_n is used to adjust the trade-off between tracking accuracy and switching effort (number of switch transitions).

$$J^*(x(k)) = \min_{u(k)} J_y(k+1) + \lambda_n \|\Delta u(k)\|_1 \quad (11a)$$

$$\text{s. t. } x(k+1) = Ax(k) + Bu(k) \quad (11b)$$

$$y(k+1) = g(x(k+1)) \quad (11c)$$

$$u(k) \in \{-1, 0, 1\}^3, \max |\Delta u(k)| \leq 1, \quad (11d)$$

with $J_y(\ell) = (T_{e,\text{ref}} - T_e(\ell))^2 + (\Psi_{s,\text{ref}} - \Psi_s(\ell))^2$, the stator flux magnitude Ψ_s and $g(\cdot)$ being the same nonlinear function as in the previous section.

Varying λ_n between 0 and 0.02, and choosing sampling intervals between $25 \mu\text{s}$ and 1ms led to the trade-off curves shown in Fig. 6. Sampling intervals shorter than $50 \mu\text{s}$ appeared to be more effective. As previously for MPDTC, the current and torque TDD points do not always correspond to each other. Specifically, to achieve torque TDDs close to the bounding (torque versus switching losses) envelope, the current TDD tends to get large. Points in Fig. 6(b) that correspond to current TDDs exceeding 18% are indicated by dots rather than circles. As can be seen, to obtain reasonably low torque TDDs for normalized switching losses below 0.32% pushes the current TDD beyond 18%.

VIII. DISCUSSION AND CONCLUSIONS

Figs. 8 and 9 summarize the trade-offs between the current and torque TDDs on the one hand and the normalized switching losses on the other. This has been done for all control and modulation schemes considered in this paper, including FOC with PWM/SVM, FOC with OPPs, one-step predictive current and torque control, and model predictive direct current and torque control. Red (black) lines refer to predictive current (torque) control, while blue (green) lines denote FOC with PWM/SVM (OPP).

With regards to the current TDD shown in Fig. 8, MPDCC and MPDTC with long horizons achieve similar performances as OPPs, with MPDCC slightly outperforming MPDTC. When approaching six-step operation, however, both schemes outperform OPPs, as was shown for MPDCC also in [17]. Shorter horizons lead to worse current TDDs, which are between the ones resulting from PWM and OPP. One-step predictive control, particularly one-step predictive torque control, appears to be less effective than PWM. Adjusting the penalty on the flux deviations independently from the one on the torque by adding a corresponding tuning parameter to the objective function is expected to enhance the performance of the one-step predictive torque controller.

When considering the torque TDD, see Fig. 9, MPDCC with the long horizon is not dissimilar to PWM, while MPDTC

⁵Unlike here, the commutations are not minimized in [12]. Moreover, this scheme was proposed for a two-level inverter only. Yet, extending it to multi-level inverters is conceptually straightforward as shown here.

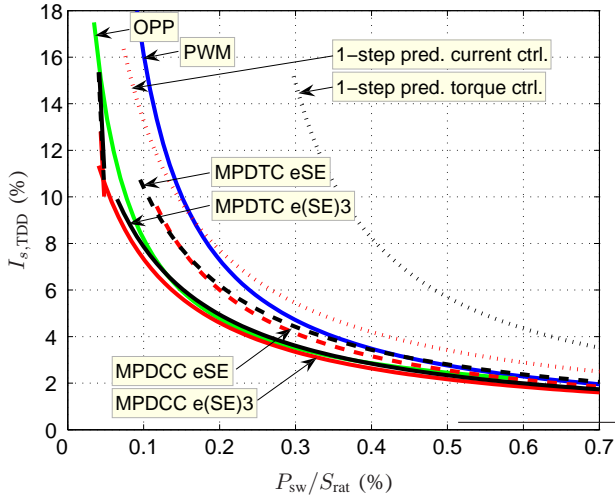


Figure 8: Comparison of the current distortion versus normalized switching losses trade-off curves for the investigated control and modulation schemes

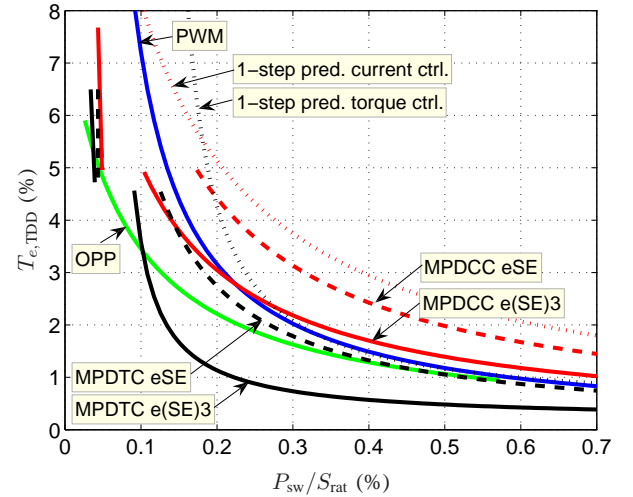


Figure 9: Comparison of the torque distortion versus normalized switching losses trade-off curves for the investigated control and modulation schemes

allows for a large reduction of the torque TDD, thus significantly surpassing OPPs, with long horizons being particularly powerful. Yet, these improvements come at the expense of inferior current TDDs. Close to six-step operation, MPDCC and MPDTC perform similarly well as the OPP. For medium to high switching losses, one-step predictive torque control matches the PWM performance with regards to the torque TDD, while it is clearly inferior for low switching losses. In terms of torque TDD, one-step predictive current control appears to be consistently inferior to PWM.

Not surprisingly, predictive control schemes that focus on the current in the objective function tend to excel at reducing the current distortions, and—to a lesser extent—also reduce the torque distortions, since low current distortions also imply low torque distortions. The converse, however, does not necessarily hold. The differences between the control approaches are pronounced at low switching frequencies and losses, while for high switching losses, the schemes tend to converge to the PWM trade-off curve.

These results are effectively independent of the machine and inverter parameters used, since only the *relative* performance of the schemes matters in this comparison. For a machine with a smaller leakage inductance for example, the *absolute* TDD values would be higher, thus stretching the trade-off curves vertically. Yet, the percentage-wise (relative) differences between the curves would remain the same.

In this paper, the performance of the different control and modulation schemes was investigated only at steady-state operating conditions. With regards to the dynamic behavior during transients and torque steps, predictive control schemes tend to be at least as fast as FOC, as shown for example in [13] and [11].

If required, additional control objectives can be easily addressed by predictive controllers, by adding them to the controller's objective function. The balancing of the neutral point potential(s) in multi-level inverters, for example, was shown for MPDTC [13], MPDCC [17] and one-step predictive

current control [11]. The compensation of the controller's computational delay is also straightforward, see e.g. [12] and [14], and is standard practice when implementing MPC schemes.

Clearly, MPDCC and MPDTC with long horizons are computationally very expensive and challenging to implement, despite the ever increasing computational power available today. As a result, MPDTC was implemented and tested on a 2 MVA drive for a short prediction horizon of about 20 time-steps only [14]. Nevertheless, it is expected that methods from mathematical programming such as branch and bound will also enable the successful implementation of MPC schemes with very long horizons [27]. The attractiveness of the one-step predictive control family is clearly its conceptual and computational simplicity.

However, particularly for medium-voltage drives, one might argue that the main benefit of new predictive control schemes is the performance improvement they bring when compared to traditional schemes such as FOC with PWM/SVM and DTC. To achieve this, it appears that long prediction horizons are mandatory to enable the optimizer to make well-informed decisions when choosing the next switching state. In fact, in a practical drive setting, the performance of new predictive control schemes might match, if not surpass, the performance of OPPs, since online optimization offers greater versatility to adapt to changing operating conditions, parameter changes, predicted disturbances or even faults than offline computed pulse patterns. Even more importantly, predictive control schemes provide the optimal switching pattern also during transients, while OPPs fail to do so, as they were computed assuming steady-state operating conditions. By contrast, short prediction horizons appear to be often less effective than established methods. To ensure the adoption of new control and modulation schemes by industry, conceptual and computational simplicity alone—as heralded by some of these new methods—might not suffice.

ACKNOWLEDGMENT

The author would like to thank Stefan Schröder for the inspiring discussions, Jan Poland for sharing his optimization package based on locally weighted regression, Georgios Papafotiou for providing the OPPs, Frederick Kieferndorf for help with the implementation of the SVM and ABB Corporate Research Switzerland for a research grant.

REFERENCES

- [1] K. H. J. Chong and R.-D. Klug. High power medium voltage drives. In *Proc. IEEE Int. Conf. on Power Sys. Techn.*, pages 658–664, Singapore, Nov. 2004.
- [2] F. Blaschke. A new method for the structural decoupling of ac induction machines. In *IFAC Symposium*, pages 1–15, Oct. 1971.
- [3] I. Takahashi and T. Noguchi. A new quick response and high efficiency control strategy for the induction motor. *IEEE Trans. Ind. Appl.*, 22(2):820–827, Sep./Oct. 1986.
- [4] R. Kennel, A. Linder, and M. Linke. Generalized predictive control (GPC) – ready for use in drive applications? In *Proc. IEEE Power Electron. Spec. Conf.*, pages 1839–1844, Vancouver, Canada, 2001.
- [5] T. Geyer. *Low Complexity Model Predictive Control in Power Electronics and Power Systems*. PhD thesis, Automatic Control Laboratory ETH Zurich, 2005.
- [6] P. Cortés, M. P. Kazmierkowski, R. M. Kennel, D. E. Quevedo, and J. Rodríguez. Predictive control in power electronics and drives. *IEEE Trans. Ind. Electron.*, 55(12):4312–4324, Dec. 2008.
- [7] D. Q. Mayne, J. B. Rawlings, C. V. Rao, and P. O. M. Scokaert. Constrained model predictive control: Stability and optimality. *Automatica*, 36(6):789–814, Jun. 2000.
- [8] S. J. Qin and T. A. Badgwell. A survey of industrial model predictive control technology. *Control Engineering Practice*, 11(7):733–764, Jul. 2003.
- [9] A. Linder and R. Kennel. Model predictive control for electrical drives. In *Proc. IEEE Power Electron. Spec. Conf.*, pages 1793–1799, Recife, Brasil, 2005.
- [10] S. Mariethoz, A. Domahidi, and M. Morari. Sensorless explicit model predictive control of permanent synchronous motors. In *Proc. IEEE Int. Electr. Mach. and Drive Conf.*, pages 1492–1499, Miami, Florida, USA, May 2009.
- [11] R. Vargas, P. Cortés, U. Ammann, J. Rodríguez, and J. Pontt. Predictive control of a three-phase neutral-point-clamped inverter. *IEEE Trans. Ind. Electron.*, 54(5):2697–2705, Oct. 2007.
- [12] H. Miranda, P. Cortés, J. I. Yuz, and J. Rodríguez. Predictive torque control of induction machines based on state-space models. *IEEE Trans. Ind. Electron.*, 56(6):1916–1924, Jun. 2009.
- [13] T. Geyer, G. Papafotiou, and M. Morari. Model predictive direct torque control – part I: Concept, algorithm and analysis. *IEEE Trans. Ind. Electron.*, 56(6):1894–1905, Jun. 2009.
- [14] G. Papafotiou, J. Kley, K. G. Papadopoulos, P. Bohren, and M. Morari. Model predictive direct torque control – part II: Implementation and experimental evaluation. *IEEE Trans. Ind. Electron.*, 56(6):1906–1915, Jun. 2009.
- [15] T. Geyer. Generalized model predictive direct torque control: Long prediction horizons and minimization of switching losses. In *Proc. IEEE Conf. on Decis. and Control*, pages 6799–6804, Shanghai, China, Dec. 2009.
- [16] J. C. Ramirez Martinez, R. M. Kennel, and T. Geyer. Model predictive direct current control. In *Proc. IEEE Int. Conf. on Ind. Techn.*, pages 1808–1813, Viña del Mar, Chile, Mar. 2010.
- [17] T. Geyer. Model predictive direct current control for multi-level inverters. In *Proc. IEEE Energy Convers. Congr. Expo.*, pages 4305–4312, Atlanta, USA, Sep. 2010.
- [18] J. Song-Manguelle, S. Schröder, T. Geyer, G. Ekemb, and J.-M. Nyobe-Yome. Prediction of mechanical shaft failures due to pulsating torques of variable-frequency drives. *IEEE Trans. Ind. Appl.*, 46(5):1979–1988, Sep./Oct. 2010.
- [19] S. Mastellone, G. Papafotiou, and E. Liakos. Model predictive direct torque control for MV drives with LC filters. In *Proc. Eur. Power Electron. Conf.*, pages 1–10, Barcelona, Spain, Sep. 2009.
- [20] J. Holtz. Pulsewidth modulation – a survey. *IEEE Trans. Ind. Electron.*, 32(5):410–420, Dec. 1992.
- [21] D. G. Holmes and T. A. Lipo. *Pulse width modulation for power converters: principles and practice*. IEEE Press, 2003.
- [22] B. P. McGrath, D. G. Holmes, and T. Lipo. Optimized space vector switching sequences for multilevel inverters. *IEEE Trans. Power Electron.*, 18(6):1293–1301, Nov. 2003.
- [23] J. Holtz and J. Quan. Drift- and parameter-compensated flux estimator for persistent zero-stator-frequency operation of sensorless-controlled induction motors. *IEEE Trans. Ind. Appl.*, 39(4):1052–1060, Jul./Aug. 2003.
- [24] G. S. Buja. Optimum output waveforms in PWM inverters. *IEEE Trans. Ind. Appl.*, 16(6):830–836, Nov./Dec. 1980.
- [25] T. Geyer and G. Papafotiou. Model predictive direct torque control of a variable speed drive with a five-level inverter. In *Proc. IEEE Ind. Electron.*, pages 1203–1208, Porto, Portugal, Nov. 2009.
- [26] T. Geyer, G. A. Beccuti, G. Papafotiou, and M. Morari. Model predictive direct torque control of permanent magnet synchronous motors. In *Proc. IEEE Energy Convers. Congr. Expo.*, pages 199–206, Atlanta, USA, Sep. 2010.
- [27] T. Geyer. Computationally efficient model predictive direct torque control. In *Proc. IEEE Energy Convers. Congr. Expo.*, pages 207–214, Atlanta, USA, Sep. 2010.